UNIVERSITY *of* York

eprints@whiterose.ac.uk
https://eprints.whiterose.ac.uk/

Synergistic biomineralization phenomena created by a combinatorial nacre protein model system.

Eric P. Chang,[†1] Teresa Roncal-Herrero,[‡] Tamara Morgan,[§] Katherine E. Dunn,[§] Ashit Rao,[¥] Jennie A.M.R. Kunitake,[&] Susan Lui,[†] Matthew Bilton,[‡2] Lara A. Estroff,[&] Roland Kröger,[‡] Steven Johnson,[§] Helmut Cölfen,[¥] John Spencer Evans[†*]

[†]Center for Skeletal Biology, Laboratory for Chemical Physics, New York University College of Dentistry, New York, NY 10010 USA.

[‡]Department of Physics, University of York, Heslington, York, United Kingdom.

[§]Department of Electronics, University of York, Heslington, York, United Kingdom.

[¥]Department of Chemistry, Universitat Konstanz, Konstanz, Germany.

[&]Department of Materials Engineering, Cornell University, Ithaca, NY, USA.

ABSTRACT

In the nacre or aragonite layer of the mollusk shell there exist proteomes which regulate both the early stages of nucleation and nano-to-mesoscale assembly of nacre tablets from mineral nanoparticle precursors. Several approaches have been developed to understand protein-associated mechanisms of nacre formation, yet we still lack insight into how protein ensembles or proteomes manage nucleation and crystal growth. To provide additional insights we have created a proportionally-defined combinatorial model consisting of two nacre-associated proteins, C-RING AP7 (shell nacre, *H. rufescens*) and pseudo-EF hand PFMG1 (oyster pearl nacre, *P. fucata*) whose individual *in vitro* mineralization functionalities are well-documented and distinct from one another. Using SEM, flow cell STEM, AFM, Ca(II) potentiometric titrations and QCM-D quantitative analyses, we find that both nacre proteins are functionally active within the same mineralization environments, and at 1:1 mole ratios, synergistically create calcium carbonate mesoscale structures with ordered intracrystalline nanoporosities, extensively prolong nucleation times and introduce an additional nucleation event. Further, these two proteins jointly create nanoscale protein aggregates or phases that under mineralization conditions further assemble into protein-mineral PILP-like phases with enhanced ACC stabilization capabilities, and there is evidence for intermolecular interactions between AP7 and PFMG1 under these conditions. Thus, a combinatorial model system consisting of more than one defined biomineralization protein dramatically changes the outcome of the *in vitro* biomineralization process.

The formation of the mollusk shell is a complex process that requires the coordination of extracellular mineralization events with the synthesis and assembly of a molecular organic framework.[1,2] The result is a highly ordered biomaterial with mesoscale bulk properties that originate from nanoscale components and their individual properties.[3-5] A case in point is the nacre layer of the mollusk shell, which consists of mesocrystal aragonite that is organized into a "brick and mortar" arrangement.[5-9] These mesocrystals are nanoporous and feature a number of nanoscale structures, such as mineral bridges,[4,10] asperities,[4,11] and tablet interlocking[4,5] that enhance the material properties of the nacre.[3-11] Recent studies now show that these aragonite mesocrystals consist of ordered spherical mineral nanoparticles that are arranged into hexagonal tablets.[6,8,9,11] This strongly suggests that a nanoscale assembly process is at work during the fabrication of the nacre layer. If true, then the assembly process may also be responsible for the formation of many of the nanoscale features that enhance the structural integrity of the nacre.

Although this nanoscale assembly process is not well understood, *in vitro* studies involving individual aragonite-associated nacre proteins have shown that protein families or proteomes may play an important role not only in nanoparticle assembly,[12-19] but also in the nanoscale modification of the mineral phase that is integral to mesoscale properties.[12-19] These families include the framework, intracrystalline, and pearl/reparative proteomes[12-26] that are localized throughout the nacre layer. Recent experiments have shown that 4 representative nacre proteins (AP7,[13-15] PFMG1,[18] n16.3,[16,17] Pif97[12]) exist as intrinsically disordered, aggregation-prone species that spontaneously form hydrogels or protein phases under both low and high ionic strength conditions.[12-17] These phases have been shown to organize and assemble amorphous calcium carbonate (ACC) nanoparticles during the early stages of

calcium carbonate nucleation and control the formation kinetics of pre-nucleation clusters (PNCs), the predecessors of ACC.[12-17] Further, these protein phases modify existing calcium carbonate crystals by introducing surface texturing, regulating directional growth, and creating random nanoporosities within the crystals themselves.[12-17] Thus, individual nacre-associated proteins possess the capabilities of nanoparticle assembly and modifications that coincide with *in situ* features that are important for the formation of mesocrystal aragonite tablets.

These reductionist studies, although informative, ignore the basic fact that proteomes manage the formation of the nacre matrix. Seminal studies[20-29] of nacre-associated proteomes have clearly demonstrated the tremendous impact of protein "collectives" on the biomineralization process, with evidence of polymorph selection and hierarchical mineral crystal organization. Thus, if we are to derive a better understanding of the biomineralization process, then our focus needs to migrate towards proteomic-based experimentation. Historically, however, there have been inherent flaws in this approach. Compared to individual protein studies, proteomic studies involving several proteins lack details that are crucial for understanding protein-mediated mechanisms of biomineralization. For example, the precise identities or functions of the individual protein components, or, the proportionalities and temporal appearance and distribution of each protein over the course of the mollusk shell mineralization process, are not known or controllable.[20-29] Without this information, the biomineralization and materials science fields cannot fully grasp the events that transpire in the nano-to-mesoscale assembly and modification processes of nacre tablets.

To explore this issue, we embarked on a program that simultaneously investigates the individual and collective behavior of multiple nacre proteins within a common *in vitro* mineralization environment. For this, we created a model combinatorial system consisting of two intrinsically disordered nacre proteins, the intracrystalline shell nacre protein, AP7 (*Haliotis rufescens*, 66 AA, C-

RING domain 31-66, chemically synthesized form = cAP7)[13-15] and the pearl-associated nacre protein, PFMG1 (*Pinctada fucata*, 116 AA, pseudo-EF hand domain 61-110, bacterial recombinant form = rPFMG1)(Figure S1, Supporting Information).[18,21] The C-RING-containing cAP7 forms hydrogels that induces the formation of intracrystalline nanoporosities and nanotexturing or nanopatterning on the exposed surfaces of calcite.[14,15] In contrast, the pseudo-EF hand rPFMG1 forms hydrogels that promote multifaceted crystal formation.[18] Note that since both proteins do not co-exist *in situ* [13-15,18] we initially viewed this model system as a "negative control", i.e., hypothetically, both proteins were not expected to interact nor assist one another within the mineralization process. Using defined molar ratios of 1:1, 1:10, and 10:1, we investigated the combinatorial effect of cAP7 + rPFMG1 on *in vitro* mineralization and early events in calcium carbonate nucleation. Our findings were surprising: both proteins exhibited functional behavior at all tested stoichiometries. However, at cAP7 : rPFMG1 = 1:1, evidence of maximal cooperativity or synergy were noted in terms of crystal modifications, nucleation, and ACC stabilization. Moreover, at this particular stoichiometry we observed two unique phenomena: the occurrence of an additional ACC nucleation event and evidence of intermolecular interactions between both proteins that are further enhanced in the presence of Ca(II) ions. Thus, even though both nacre proteins originate from distinctly different nacre environments and phylogenetic origins, when combined together they become synergistic and dramatically change the outcome of the *in vitro* biomineralization process.

EXPERIMENTAL PROCEDURES

Sample preparation. The preparation and purification of chemically synthesized AP7 (cAP7, MW = 7.5 kDa)[14] and recombinant PFMG1 (rPFMG1, MW = 13.6 kDa,)[18] were performed as described previously.

In vitro micro-mineralization assays. Mineralization microassays were conducted by mixing equal volumes of 20 mM $CaCl_2*2H_2O$ (pH 5.5) and 20 mM $NaHCO_3$ / Na_2CO_3 buffer (pH 9.75 in Milli-Q Type I ultrapure water 0.22 μm filtered) to a final volume of 500 μL in sealed polypropylene tubes and incubating at room temperature for 1 hr.[13-17] Aliquots of cAP7 and rPFMG1 stock solutions were added to the calcium solution prior to the beginning of the reaction, with final assay concentrations of each protein to be either 0, 1, or 10 μM. The final pH of the reaction mixture was measured and found to be approximately 8.0 - 8.2.[13-17] Mineral and protein deposits formed during the assay were captured on 5 x 5 mm Si wafer chips (Ted Pella, Inc.) that were placed at the bottoms of the vials. Upon completion of the mineralization assay period, the Si wafers were rinsed thoroughly with calcium carbonate saturated methanol and dried overnight at room temperature prior to analysis. SEM imaging of the Si wafers extracted from the mineralization assays was performed using a Zeiss Merlin field emission SEM (FESEM) using either an Everhart-Thornley type secondary electron detector (SE2) or an annular secondary electron detector (in lens) at an accelerating voltage of 1.5kV, a working distance of 4 mm, and a probe current of 300 pA. Prior to analysis, SEM samples were coated with iridium using a Cressington 208HR sputter coater with thickness controller attachment.

Focused ion beam sectioning of crystals. Imaging of internal crystal morphology was performed using a Zeiss Auriga Small Dual-Beam FIB-SEM.[12,13] For these analyses all samples were first coated with 4 nm iridium prior to SEM imaging, then coated with 50 nm of Au prior to performing FIB. A 30 kV 120 pA gallium ion beam was oriented perpendicular to the sample by tilting the sample stage to 54˚ and utilized to mill 15 nm serial cross-sections. SEM images of cross-sectioned surfaces were then obtained using a 2.0 kV 600 pA electron beam and a secondary electron detector at a working distance of 5.0 mm. Images of surfaces containing electron beam damage were created for comparison to images of undamaged surfaces but were not used for the purposes of discussion in this publication.

Images were taken shortly after cross sectioning to limit the exposure of the uncoated surfaces to the electron beam.[12,13]

STEM liquid flow cell imaging of nano-mineralization. To monitor the dynamics of protein-mineral complex formation liquid cell scanning transmission electron microscopy (LC-STEM) experiments were performed using a three-port Poseidon 200 holder (Protochips, Inc.) in an aberration corrected JEOL 2200 FS using spot size 3C (4 pA beam current) at 200 kV and an high-angle annular dark-field (HAADF) detector.[14] For the mixing experiment 500 nm spacers and flow rates between 5 and 10 μL/hr were used. The TEM holder was flushed with the two different protein solutions, one being 4 μM cAP7 and the other 4 μM rPFMG1 dissolved in Milli-Q water; these solutions were mixed *in situ* at the tip of the liquid cell holder to study the interaction between both proteins. A second experiment involved the injection of 4 μM cAP7 in 10 mM $CaCl_2 \cdot 2H_2O$ in one of the inlet ports and 4 μM rPFMG1 in 10 mM $NaHCO_3$ in the second inlet port with mixing of the two solutions occurring in the flow cell chamber. To ensure the mixing of both solutions, a control experiment was performed by mixing equivolumetric quantities of the same solution and manually agitated it before pumping into the LC-STEM holder. This experiment confirmed that the observed aggregates observed in the first two experiments were similar to those found during the control experiment. The calcium and carbonate containing assay solutions for both protein-containing and protein-deficient assay were prepared from 20 mM $CaCl_2*2H_2O$ and 20 mM $NaHCO_3$, respectively (in Milli-Q water, final assay solution = 1:1 mixture; final pH = 8.1 – 8.3).[14]

Calcium potentiometric titrations. Potentiometric titration experiments were performed on cAP7, rPFMG1, and cAP7 : rPFMG1 (molar ratios = 1:1, 1:10, 10:1) samples at room temperature by using a computer-controlled titration system operated with the supplied software (Tiamo v2.2, Metrohm GmbH, Filderstadt Germany). The experimental set-up has been described earlier.[30-36]A polymer-based

ion-selective electrode and a flat-membrane glass electrode were used to monitor the free Ca(II) concentration and pH respectively. During a titration run, $CaCl_2$ (10 mM) solution was dosed at a constant rate of 0.01 mL/min to 10 mL of the protein solution in carbonate buffer (10 mM), which was constantly stirred at 800 rpm at room temperature. Titrations were performed at constant pH value of 9.0 that were maintained by counter-titration of NaOH (10 mM). Reference and calibration experiments were performed by dosing $CaCl_2$ (10 mM) into carbonate buffer (10 mM, pH 9.0) and water (pH 9.0), respectively.[30-38]

AFM imaging of protein phases. We investigated the dimensional and morphological characteristics of cAP7, rPFMG1, and cAP7 : rPFMG1 assemblies on mica substrates using tapping mode AFM.[12,14,17,18] Reconstituted forms of individual and 1:1 molar protein complexes were imaged as droplets on mica in 10 mM Tris-HCl buffer (pH 8.0) for protein concentrations of 1 μM. In the case of the 1:1 sample, an additional experiment was conducted in 10 mM Tris-HCl, 10 mM $CaCl_2$, pH 8.0, to mimic mineralization conditions. AFM experiments were conducted at 25 °C using an Agilent 5500 operating in tapping mode in buffer solution. Olympus AC240TS rectangular-shaped, aluminium reflex coated, silicon tips with a spring constant of approximately 2 N/m and a fluid drive frequency of ~28 kHz were used for imaging. All samples were aliquoted onto a freshly stripped surface of mica (0.9 mm thick, Ted Pella, Inc.) and incubated for a period of 15 minutes at ambient temperature prior to measurement. Images were acquired at a scan rate of 2 Hz. Gwyddion Software was implemented for image processing, noise filtering and analysis, including the calculation of R_q, i.e., the surface roughness averaged over several cross sections of the mica surface. Histogram values represent measurements taken for 30 particles at each scenario. [12,14,17,18]

QCM-D interaction studies. Quartz crystal microbalance with dissipation monitoring (QCM-D) experiments were performed using a Q-sense E4 system from Biolin Scientific. Gold-coated AT-cut

quartz sensors were used (QSX 301, Biolin Scientific), for which the fundamental frequency was 4.95 MHz +/- 50 kHz. The sensors were initially subjected to a ten minute cleaning step in a UV-ozone cleaner, with the active side facing upwards. The sensors were then placed successively in solutions of Hellmanex III (2%) and ultrapure Milli-Q water (twice), and sonicated in each bath for ten minutes, with the active side facing upwards in all instances. The sensors were then dried with N_2 gas and replaced in the UV-ozone cleaner for thirty minutes. Finally, the sensors were left to soak in 100% ethanol for approximately thirty minutes and dried with N_2 before installation in the flow modules.

The QCM-D flow chambers were flushed with ultrapure Milli-Q water before each measurement, until a stable baseline was established (< 0.5 Hz shift over 10 mins). The flow module temperature was maintained at 16 ^{O}C throughout and the flow rate was kept constant at 20 µL/min. The sensor surfaces were then functionalized with poly(L-lysine) by incubation with a 0.01% aqueous solution of poly(L-lysine) until the surface was saturated (around 20-30 minutes). The poly(L-lysine) acts as a biocompatible support for non-specific immobilization of proteins. Next, two scenarios were examined. The first involved the introduction of a 10 µM rPFMG1 solution (or 10 µM cAP7) in Milli-Q water into the QCM-D flow chambers again until saturation. Buffer salts were not utilized in this scenario as these typically induce precipitation to aggregation-prone, intrinsically disordered proteins. The second involved the introduction of a 10 µM solution of cAP7 (or 10 µM rPFMG1) dissolved in 10 mM $CaCl_2$ solution in Milli-Q water. Here, we expect that pre-aggregation of the flow-introduced protein occurs in the presence of Ca(II) prior to interactions with the adsorbed protein layer.

RESULTS

cAP7 and rPFMG1 jointly form unique "pinecone" calcite crystals. This initial study focused on protein-mediated events that occur within *in vitro* calcite nucleation assays since these are highly reproducible.[12-18] As described earlier, the choice of cAP7 and rPFMG1 for these combinatorial studies arises from the unique mineralization "signatures" that each protein exhibits within these assay systems (cAP7 = surface nanotexturing; rPFMG1 = multifaceted crystal formation)(Fig 1A, B).[13-15,18] This allows us to monitor the participation of each protein within our mineralization microassay system and allows comparisons of nacre protein functionality and aggregation phenomena in 60 min or less,[12-18] and thus serves as a robust platform for comparing cAP7, rPFMG1, and cAP7 : rPFMG1 combinations side-by-side.

When both proteins are present together combinatorial effects are seen that scale with the proportionality of each protein (Fig 1C-E). At 1:1 molar ratio, unique mesoscale calcite crystals predominate in the assays, which we denote as "pinecone" structures (Fig 1C), and these exhibit variation in morphology and degree of nanopatterning (Fig S2, Supporting Information). Using microRaman spectroscopy we confirmed these pinecone structures to be calcitic in nature (Fig S3, Table S1, Supporting Information), which explains the presence of angular features. These pinecones are circular to ellipsoidal in cross-section and at higher magnification we note the presence of nanopatterning or nanotexturing on the surfaces of each crystal (Fig S2, Supporting Information). Our interpretation of the 1:1 scenario is that rPFMG1 and cAP7 are jointly creating nanopatterning[14,15] at the surface, with the net result being unique nanotexturing effects that are not observed for the individual proteins themselves (Fig 1F, G). When we examine scenarios when each protein is predominant over the other (cAP7 : rPFMG1 = 1:10; 10:1), the effects on crystal morphology scale appropriately, i.e., the predominant protein controls the scenario and the subdominant protein contributes its share (Fig 1D,

E).   Hence, each nacre protein exerts its individual functionality over the tested stoichiometry range, but at the 1:1 stoichiometry scenario unique effects are seen on crystal growth.
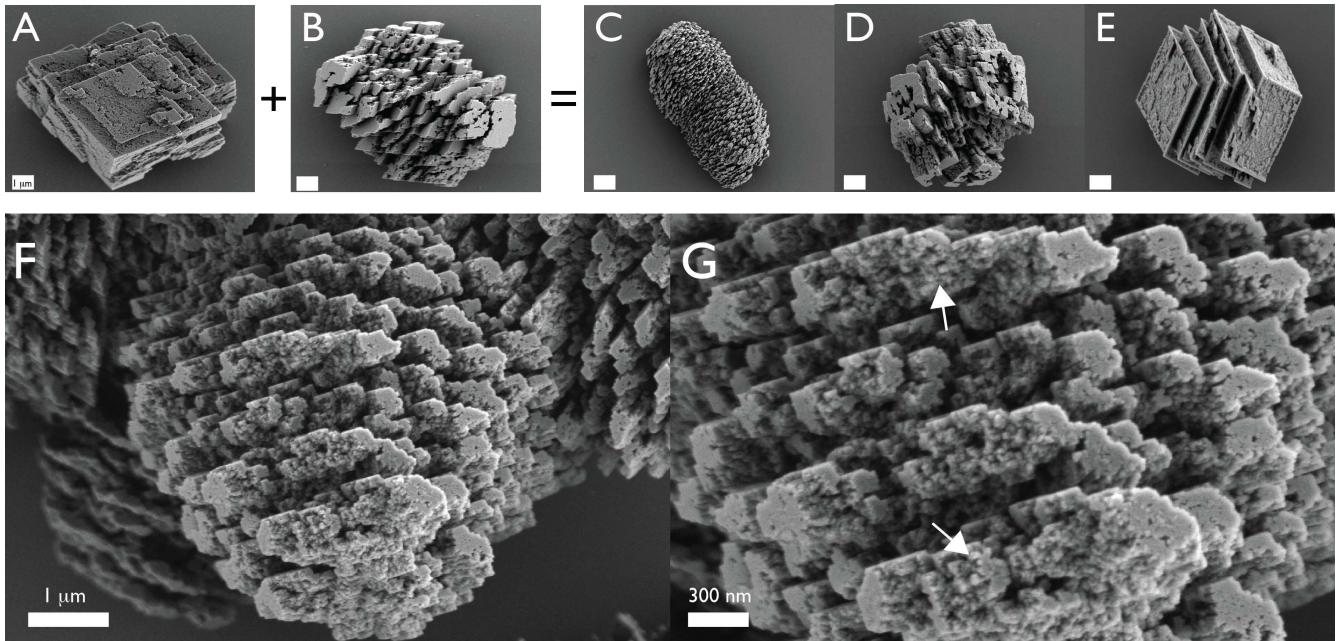

Figure 1. SEM images of calcite crystals generated in the presence of (A) cAP7, (B) rPFMG1, (C) 1:1 rPFMG1 : cAP7, (D) 10:1 rPFMG1 : cAP7; (E) 1:10 rPFMG1 : cAP7. Images (F) and (G) are high magnification images of 1:1 rPFMG1 : cAP7 "pinecone" morphologies which reveal nanotexturing and nanopatterning (denoted by white arrows). For A,B,C,F,G, the final concentration of each protein is 10 µM. In D, E the predominant protein is 10 µM and the subdominant protein is 1 µM. In A-E, scalebars = 1 µm. Other "pinecone" morphologies can be found in Supporting Information, Fig S2.

The 1:1 scenario generated very interesting results, and given that the unique surfaces of the pinecone structures might entrap protein aggregates or hydrogels and incorporate these within the mineral overgrowth phase,[12,15,16] we focused on these crystals for subsequent subsurface analysis. Using FIB-SEM we sectioned the pinecone crystals and discovered the presence of intracrystalline nanoporosities (Fig 2). Previous studies with AP7 documented the formation of random nanoporosity formation at the peripheral intracrystalline regions of calcite crystals that came into contact with cAP7 protein phases.[13,15] In the case of rPFMG1, nanoporosities or voids are observed at the surface of the
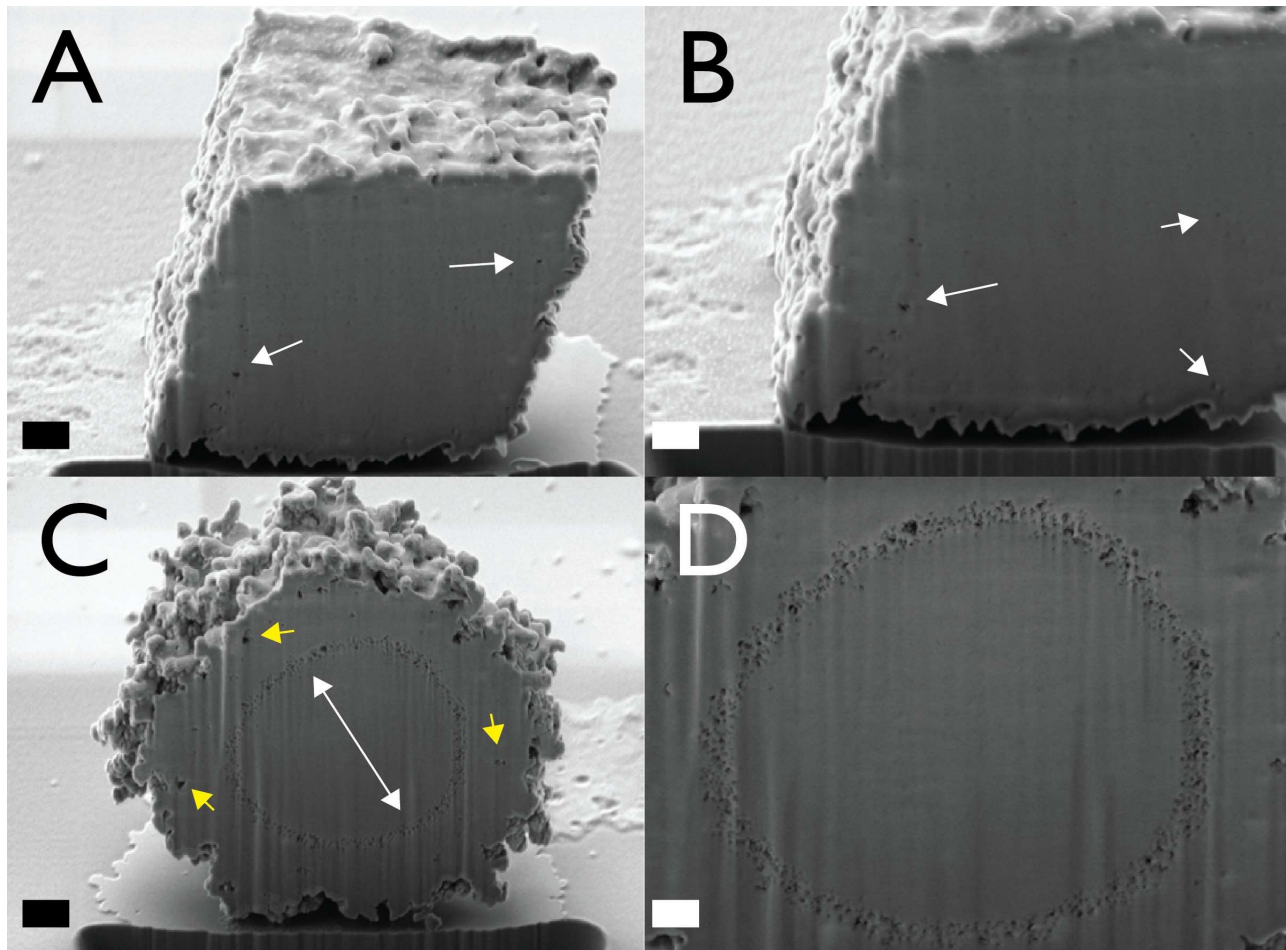
Figure 2. SEM images of FIB-sectioned calcite crystals. (A, B) Typical protein-deficient assay calcite crystal (60 minutes assay time), which features minimal porosities (white arrows). (C,D) Representative calcite "pinecone" crystals generated in assays containing 1:1 cAP7 : rPFMG1 (10 μM each), where one can clearly denote multiple subsurface void or pore regions (yellow arrows) and internal annular-arrangements (white arrows). Scalebars = 200 nm.

crystal clusters (Fig 1B) with no discernible arrangement.[18] However, as shown in Fig 2, the pinecone

features two kinds of intracrystalline nanoporosities. The first kind are located at the periphery and

appear random in size and distribution. These are termed "peripheral" nanoporosities and we believe

that these formed as a result of the topographical convolutions of the pinecone which may have

entrapped surface-deposited protein aggregates that later formed voids as mineral overgrowth proceeds,

similar to what occurs in the presence of crystal-adsorbed AP7 protein hydrogels.[13,15] The second kind

are centrally localized within the pinecone crystals and feature an annular distribution or arrangement.

We denote these as "annular" nanoporosities. Given that macromolecular-induced intracrystalline

nanoporosities observed in biogenic calcite[12,13,15,16,39,40] and nacre aragonite tablets[4-11,41] are randomly-distributed, the formation of spatially ordered nanoporosities by the "mini-proteome" (Fig 2) was unexpected and unique. We believe that the annular porosities represent surface-deposited protein aggregates that became incorporated[13,15] at a timepoint earlier than the "peripheral" type, as we will elaborate upon in the Discussion section. Thus, in addition to creating unique crystal morphologies, the 1:1 cAP7 : rPFMG1 combination also alters the appearance and distribution of intracrystalline nanoporosities within calcium carbonate crystals *in vitro*.

CAP7 + rPFMG1 alters non-classical nucleation and creates a secondary nucleation event. Our focus now shifts to earlier *in vitro* mineralization events which involve the formation of pre-nucleation clusters (PNCs) and their transformation into amorphous calcium carbonate (ACC) occurs, i.e., the non-classical nucleation scheme.[30-36] To determine the effect that both nacre proteins have on this *in vitro* process, we conducted calcium potentiometric experiments at pH 9.0 to minimize bicarbonate ion formation, subsequent outgassing, and pH shift artifacts.[14,17, 30-36] When we examine the individual protein titration dataset we find the following: a) the time interval for the nucleation of calcium carbonate clusters is 15% longer for rPFMG1 than cAP7 (Fig 3A; Fig S4, Table S2, Supporting Information), b) As evidenced by the linear slope of the titration curve relative to the control scenario, cAP7 has very little effect on PNC stability, but rPFMG1 stabilizes PNCs, (Fig 3B; Fig S4, Table S2, Supporting Information); c) rPFMG1 exhibits a more significant effect (i.e., factor of 2 or greater) towards initially nucleated precursor phases compared to cAP7 (Table S2, Supporting Information). Overall, PFMG1 > cAP7 with regard to PNC and ACC stabilization.

Intriguingly, when we examine cAP7 and rPFMG1 together, a different picture emerges. At cAP7 : rPFMG1 = 1:10, 10:1, and 1:1 (Fig 3A, B; Fig S5, Table S2, Supporting Information), the
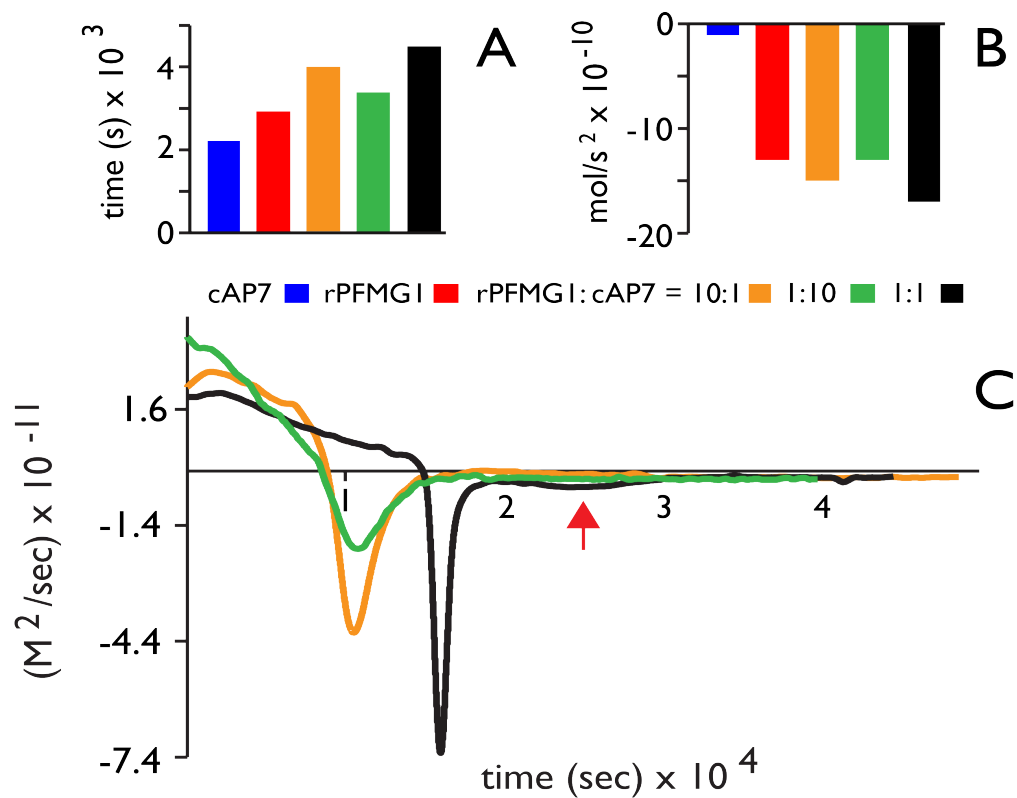
Figure 3. Potentiometric titrations of cAP7, rPFMG1, and cAP7 : rPFMG1 (1:1, 10:1, 1:10) (A) Histogram plot of control-corrected nucleation times; (B) Histogram plot of control-corrected pre-nucleation slope values (i.e., PNC stabilization); C) Time-dependent ACC solubility plot (ΔSolubility / ΔTime). The second ACC nucleation event is denoted by the red arrow. The presented values are subtracted with corresponding values from reference titrations. Note that Figure 3C shows the change in solubility product per unit time and does not directly refer to the absolute values. The absolute values are presented in Table S2 (Supporting Information) which show a significant change in solubility from $10*10^{-8}$ to $3*10^{-8}$ M^2.

nucleation times and PNC stabilization effects are observed to be greater than those observed for the individual proteins, with the most significant effects obtained at 1:1. The effects observed here are significant as compared to previous publications,[37,38] wherein titration assays were used to test the effect of several additives in a high throughput manner. For instance, the magnitude of prenucleation slope change is $\sim 10*10^{-10}$ mol/sec for nacre proteins (Table S2, Supporting Information) whereas monosaccharides generally can induce a slope change of about $2\text{-}3*10^{-10}$ mol/sec.[37]

But the most interesting feature is the number of nucleation events (Fig 3C; Table S2, Supporting Information). At cAP7 : rPFMG1 = 1:10 or 10:1, there is only a single nucleation event corresponding to amorphous forms of calcium carbonate and the stabilization effects coincide with the predominant protein species (i.e., rPFMG1 > cAP7). But at cAP7 : rPFMG1 = 1:1, the original ACC nucleation event shifts to a later time period and exhibits greater ACC stabilization overall (i.e., increased minima). Additionally, we note the appearance of a second nucleation event (red arrow, Fig 3C, 10 μM cAP7 : 10 μM rPFMG1; Fig S5, Table S2, Supporting Information) that is lower in stability and broader in time interval compared to the initial nucleation event. Similarly, a dual nucleation event was also observed at lower protein concentrations (i.e., 1 μM cAP7 : 1 μM rPFMG1) albeit with weaker intensity (Fig S5, Table S2, Supporting Information). Note that a second nucleation event was not detected at 1:10, 10:1, nor observed for the individual proteins themselves. The presence of a second nucleation event in potentiometric experiments is significant, since it is indicative of the presence of a transient polymer-induced liquid precursor (PILP) or highly hydrated amorphous phase that initially forms, then gradually transforms into ACC. This gradual transformation would explain the weaker intensity and broad time transition of the second event (Fig 3C, red arrow).[42-45] Thus, at 1:1 cAP7 : rPFMG1, we believe that the two proteins combine to form a PILP-like or highly hydrated phase that stabilizes the nucleation process to a greater extent than either cAP7 and rPFMG1 alone, and allows for the gradual formation of ACC over time.

STEM flow cell imaging of 1:1 cAP7:rPFMG1 protein and mineral phases. If cAP7 and rPFMG1 combine with mineral precursors to form a PILP-like phase at 1:1 stoichiometry under mineralization conditions (Fig 3C), then we would expect to see some evidence of a stabilized protein aggregate, phase, or hydrogel in the presence of a stabilized amorphous mineral phase (ACC). To test this, we

utilized STEM flow cell imaging techniques to examine two scenarios (Fig 4): (1) 1:1 cAP7 : rPFMG1 in pure water (i.e., 0.2 μm filtered Milli-Q grade water, which minimizes protein aggregation);[12,14,46] (2) 1:1 cAP7 : rPFMG1 under mineralization conditions at pH 8.0. We chose 4 μM concentrations for both proteins based upon our previous mineral assembly studies with cAP7 in the STEM flowcell apparatus.[14] Note that once counterions are introduced, even at low concentrations (i.e., < 1 mM), the charged residues of intrinsically disordered proteins form ion pairs with the corresponding ions, which changes protein solubility and promotes protein-protein interactions to stabilize polypeptide chains. One should note that the limited volume (i.e., nL), the gradual introduction of one protein component with another, and beam heating issues are unique to the STEM flowcell experiments[14] and thus drawing direct comparisons to larger volume, room temperature microliter microassay results (Fig 1) is not feasible.

In the first scenario, we started with cAP7 in the flow cell and introduced the rPFMG1 sample over time (0-130 min), reaching a 1:1 protein stoichiometry (Fig 4, top panel). Initially, angular cAP7 nanoparticles are observed (60 min), similar to what we originally noted in previous cAP7 AFM studies at pH 8.0, and this indicates that under pure water conditions[46] cAP7 is aggregating within the STEM flowcell as expected.[14] As rPFMG1 is introduced these angular particles give way to larger, amorphous-appearing dense mesoscale protein phases (at 80, 130 min), which remain stable over time. Our interpretation is that rPFMG1 is co-aggregating with cAP7 to form a hybrid protein phase. In the second scenario we repeated this experiment in the presence of 10 mM Ca(II) and HCO_3- solutions (Fig 4, bottom panel). Here, we note the rapid formation of dense, mesoscale protein phases (10 min) and the presence of numerous electron-dense, amorphous-appearing nanoscale mineral phases, presumably ACC, within the boundaries of the protein phase. We also observe larger electron-dense particles that
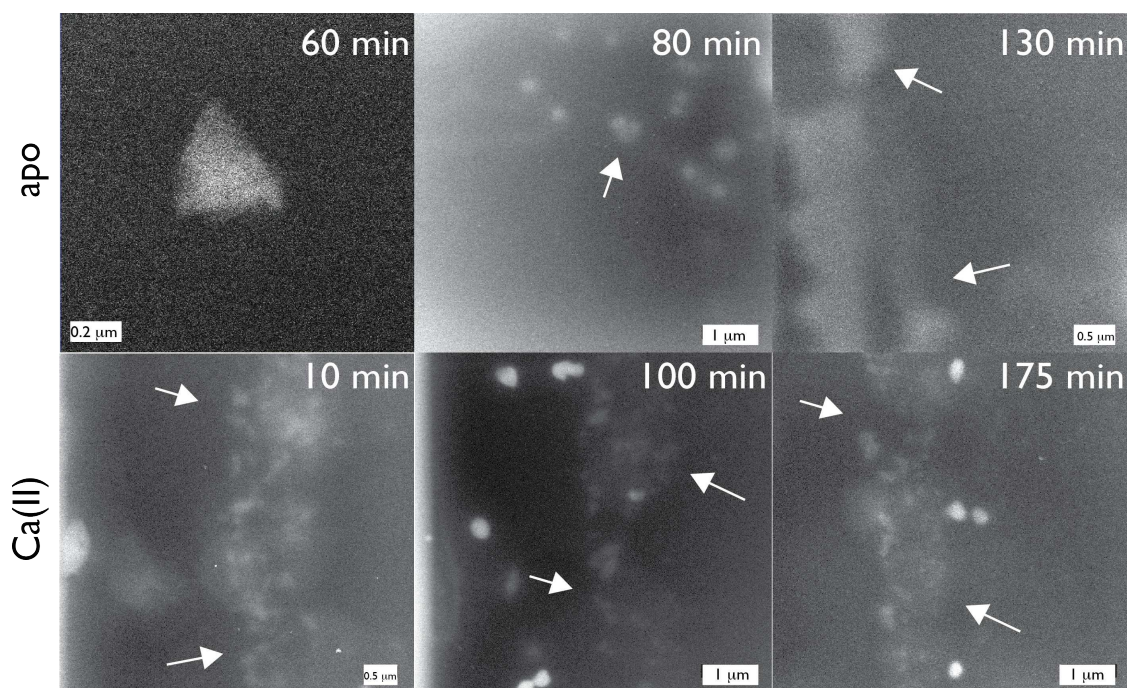
Figure 4. STEM video stills of (A) protein phase formation in Milli-Q water; (B) protein and mineral phase formation in 10 mM calcium carbonate solutions. For (A), 10 μM cAP7 is initially in the flow cell and the representative image was taken 60 min post-injection of the 10 μM rPFMG1 solution. At this timepoint we can detect angular cAP7 protein complexes in the flowcell. As time evolves, the protein complexes become larger in size and develop an amorphous appearance in the flowcell. In (B), the same protein phase formation process is observed, with the simultaneous appearance of round, amorphous-appearing mineral nanoparticles that are associated with the protein phase. Note that in the protein-deficient experiments mineral nanodeposits are first observed at 20 min post-injection of the calcium solution and evolves much more rapidly (i.e., < 60 sec) and without organization.[14]

appear to be distinct from the protein phase. As shown in Fig 4, the mineral and protein phases appear to be very stable (up to 175 min) and we do not observe the formation of a crystalline mineral phase (i.e., appearance of angular deposits) within the flowcell during the course of these experiments. As described in our previous STEM flow cell studies of cAP7, in the protein-deficient control scenario calcium carbonate nanoparticles start to appear at 20 min post-mixing and feature amorphous morphologies.[14] These particles rapidly grow over a 30 sec period. Thus, the rate of mineral nanoparticle formation is much faster in the protein-deficient scenario than what we observe in the presence of 1:1 cAP7 : rPFMG1 (Fig 4).[14] In conclusion, our STEM visualization studies confirm that the 1:1 stoichiometric condition generates mesoscale protein phases or hydrogels that associate with and

stabilize ACC nanoparticles, which correlates with a PILP-like phase that we detected in our calcium potentiometric experiments (Fig 3C, Table S2, Supporting Information).[42-45]

Evidence of synergistic aggregation and intermolecular protein interactions. We further confirmed the formation of protein phases or aggregates at cAP7 : rPFMG1 = 1:1 using tapping mode AFM imaging techniques (Fig 5). At pH 8.0 (10 mM Tris), both cAP7 and rPFMG1 individually form protein nanoaggregates on fresh mica surfaces, with the particle dimensions (height, diameter) and surface roughness (or R_q factor, which is indicative of protein film formation on mica) of cAP7 exceeding those of rPFMG1 by 30% and 10%, respectively (Fig 5a,b,e).[14,18] At 1:1 stoichiometry we note the formation of amorphous protein aggregates on mica surfaces; these aggregates possess morphologies, increased dimensions (+20-30%), and larger R_q parameters (+40-50%) which diverge from cAP7 and rPFMG1values (Fig 5c,e) and suggest that a hybrid protein aggregate or phase has formed. When the 1:1 scenario is imaged in the presence of Ca(II), we witness an increase in protein aggregate dimension, R_q values, and morphologies (Fig 5d,e) that are very distinct from any of the other tested scenarios (Fig 5a-c). Note that individual nacre protein phases such as those generated by cAP7[14] and rPFMG1[18] also show dimensional increases in Ca(II) buffers. Thus, 1:1 cAP7 : rPFMG1 forms large, dense amorphous-appearing assemblies on mica that are distinctive from those formed by the individual proteins, not unlike the dense phases we observed in the STEM flow cell (Fig 4) under pure water and mineralization conditions.

From the foregoing, it is possible that cAP7 and rPFMG1 proteins may be forming hybrid cAP7-rPFMG1 aggregates, i.e., there are intermolecular interactions taking place between both nacre proteins under low ionic strength and mineralization conditions. To probe for cAP7 – rPFMG1 protein interactions we utilized a QCM-D system and mimicked the approached utilized in our STEM flow cell
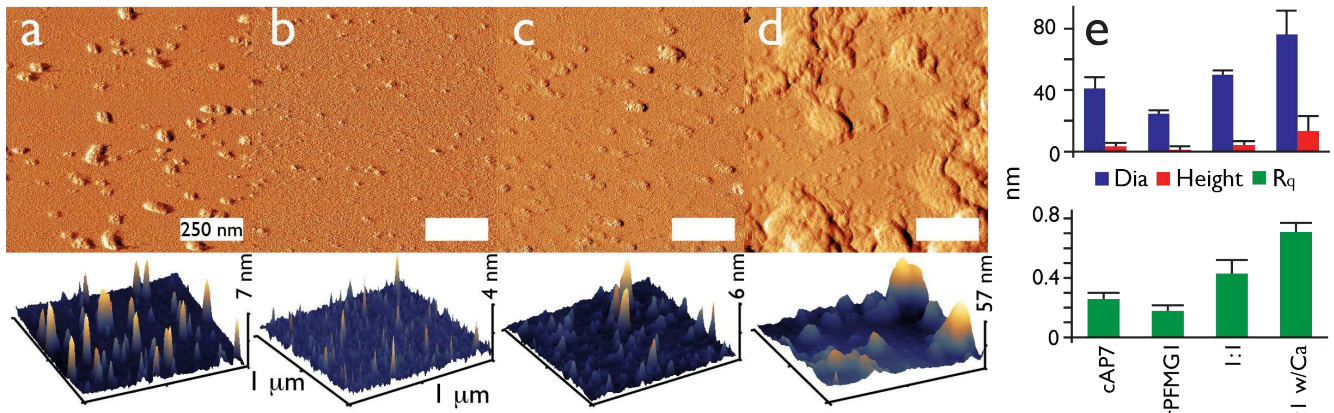
Figure 5. AFM tapping mode imaging of nacre protein phases on freshly cleaved mica surface, 10 mM Tris-HCl, pH 8.0. (a) 1 μM cAP7; (b) 1 μM rPFMG1; (c) 1:1 cAP7 : rPFMG1 (1 μM each) (d) as per (c) but in the presence of 10 mM $CaCl_2$, 10 mM Tris-HCl, pH 8.0. (e) Histogram plots of mean particle diameters, heights, and R_q values ($\pm$ S.D.) obtained from the datasets described in (a) through (d). Histogram values represent measurements taken for 30 particles at each scenario.[12,14,17,18]

studies, i.e., we started with one protein immobilized on the surface of an Au-coated QCM-D sensor placed in a flow module and introduced the second protein over time. Note that this approach cannot replicate the 1:1 proportionality scenario we employed in our flow cell STEM experiments (Fig 4) since we are immobilizing one protein onto the sensor first then introducing the second protein, rather than mixing them together in a predetermined ratio. Thus, we are merely measuring the interaction of the free protein component with the immobilized protein component. The QCM-D experiments were conducted under two conditions: in 0.2 μm filtered Milli-Q grade water (to minimize overall aggregation of aggregation-prone intrinsically disordered proteins)[46] and then under conditions containing 10 mM $CaCl_2$ to mimic mineralization conditions without interference from ACC or calcite precipitation (Fig 6). Note that in the latter instance Ca(II) ions will promote aggregation of either protein[14,18] and thus pre-aggregation of the flow-introduced protein component will occur prior to interaction with the surface-adsorbed protein component. In these studies, poly(L-lysine)-coated Au QCM-D sensors were utilized to provide a biocompatible surface for initial protein adsorption (note

that both cAP7 and rPFMG1 contain Asp, Glu residues (Fig S1, Supporting Information)[14,18] and thus

should be electrostatically compatible with poly(L-lysine) coatings).
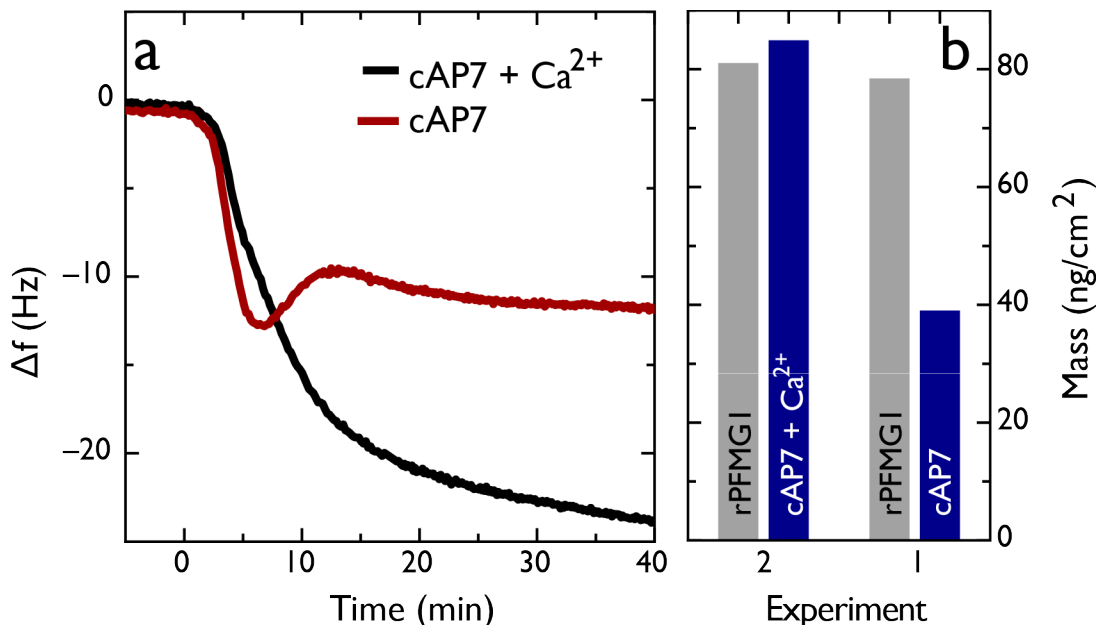

Figure 6. QCM-D experiments conducted on cAP7 and rPFMG1 (10 μM each). (a) QCM-D data showing decrease in resonant frequency (thus increase in mass) when exposing a layer of rPFMG1 to either cAP7 or cAP7 in the presence of 10 mM CaCl$_2$. (b) Histograms showing mass of rPFMG1 was approximately the same in both channels but significantly greater mass of cAP7 deposited in the presence of Ca(II) ions (Experiment 2) as opposed to the apo-state [i.e., no Ca(II), Experiment 1].

As shown in Fig 6a and Fig S6 (Supporting Information), in this specific example we created a

layer of adsorbed rPFMG1 protein on poly(L-lysine) with a density approximating 3.5×10^{12}

proteins/cm^2 (calculated using the Sauerbrey equation and the 5th overtone), which is typical of a

surface immobilized protein layer. When this rPFMG1 protein layer is exposed to cAP7 in either pure

water or 10 mM CaCl$_2$, there is a noted decrease in resonance frequency, or Δf, consistent with an

increase in immobilized mass. We also tested the reverse scenario (i.e., cAP7 adsorbed onto poly(L-

lysine), rPFMG1 introduced via flow) and found that both proteins still exhibited interactions (Fig S7,

Supporting Information), thus confirming that cAP7 interacts with rPFMG1 under low ionic strength

conditions and in the presence of Ca(II). Thus, although cAP7 and rPFMG1 originate from different

tissue sources and mollusks, there are detectable interactions between both proteins at 1:1 stoichiometry, which would explain the formation of PILP-like phases (Figs 4, 5).

Two other phenomena of interest are noted. First, we observe a peak in the cAP7 curve (Fig 6a), i.e., the frequency and dissipation change non-monotonically. Similar phenomena were observed in QCM-D studies of vesicles forming lipid monolayers.[47] Here, an increase in mass and dissipation were noted as the vesicles adsorb to the surface followed by a loss in mass and decrease in viscoelasticity when they rupture, where the loss in mass is associated with the loss of water from the vesicle.[47] We postulate that a similar effect occurs cAP7 – rPFMG1 binding, i.e., there is an initial increase in mass and viscoelasticity followed by a loss in mass due to water and a corresponding decrease in dissipation. During this process conformational changes may be occurring in either the rPFMG1 or cAP7 layer that arise from changes in layer density, or changes in the intrinsic disorder content of the protein molecules (i.e., increase in disorder due to denaturation, or induced folding due to protein-protein interaction).[48-52] Second, the degree of interaction between cAP7 and rPFMG1 is calcium-dependent: as presented in Fig 6, the mass increase is approximately 50%, for cAP7 in water but for cAP7 in the presence of Ca(II) the mass increase is around 100%. This finding is also confirmed in Fig 6b where we note the mass of rPFMG1 was the same in both experiments but a significantly greater mass of AP7 adsorbed onto the rPFMG1 layer in presence of Ca(II) ions. As mentioned earlier, we believe these enhanced interactions may be due to increased aggregation of the cAP7 component within the Ca(II) solution; however, we cannot rule out the possibility that Ca(II) ions are somehow enhancing the interactions between cAP7 and rPFMG1, thereby increasing the adsorption and observed mass.

DISCUSSION

For the first time a pair of mollusk shell nacre proteins with defined characteristics have been combined within test *in vitro* scenarios where the molar proportionality of one protein is varied relative to the other. A key finding of this study is that the C-RING AP7 and pseudo-EF hand PFMG1, although originating from different proteomes and organisms, are functionally active within defined mixtures (Figs 1-4). Even at ratios where the content of one protein predominates over the other (i.e, 1:10, 10:1), one can still see the mineralization "signature" of each protein contributing to the overall mineralization events *in vitro* (Figs 1-4). However, the net mineralization "signature" of the mixtures is distinctly different from that of the individual proteins themselves as evidenced in both the early (Fig 3, 4) and later (Figs 1, 2) stages of calcium carbonate nucleation *in vitro*. This suggests that both proteins can functionally co-exist within the same standardized assays and the predominant protein does not significantly impair the functionality of the minority protein in either scenario. Thus, the cAP7-rPFMG1 combination is functional and will be used as model system to study multiple protein-mediated biomineralization phenomena *in vitro*.

One of the most interesting findings are the nucleation and crystal growth events that occur at 1:1 cAP7 : rPFMG1 stoichiometry (Figs 1-4). Here, we believe that the functionalities of both proteins synergistically combine to alter the outcome of the *in vitro* nucleation process in a manner that diverges from other ratios and from the individual proteins themselves. We will first discuss our findings within the context of the earliest stages of the mineralization process (Figs 3,4; Table S2, Supporting Information). Within the non-classical nucleation scheme, the 1:1 cAP7 : rPFMG1 mixture (10 μM : 10 μM) significantly extends the time interval for PNC formation by 50% and 46% over that induced by the individual cAP7 and rPFMG1 proteins, respectively, and 36-40% over the 1:10 and 10:1 scenarios

as well (Fig 3A,B; Table S2, Supporting Information). Similarly, PNC stability (i.e., slope of the linear prenucleation regime) increases by 23% - 107% in the 1:1 scenario compared to the individual proteins. Most importantly, the 1:1 cAP7 : rPFMG1 scenario promotes a second nucleation event (Fig 3C) where a more soluble mineral phase forms over a more extended time period compared to the initial nucleation event. The presence of two nucleation events has been documented in potentiometric systems where polymers or polypeptides and amorphous mineral phases combine to form PILP.[34,42-45] Thus, in the 1:1 scenario, we believe that the cAP7 and rPFMG1 have synergistically formed a PILP-like phase with the mineral components during the early stages of the *in vitro* nucleation process.

We will now consider the impact of the 1:1 scenario at later stages of nucleation (Fig 1, 2). Here, we witness an unusual combination of nanopatterning, nanotexturing (Fig 1), and the presence of organized intracrystalline nanoporosities (Fig 2). The nanotexturing effects have been witnessed in other nacre protein systems, such as AP7[13,15] and n16.3,[16,17] where protein phases form in the mineralization assay solution, randomly deposit and contact the forming mineral surface, and modify nucleation. We believe that a similar process occurs in our microassays (Fig 1). Similarly, AP7, Pif97, and n16.3 nacre protein phases which deposit onto crystal surfaces have been implicated in the formation of randomly-distributed subsurface nanoporosities within *in vitro* calcite crystals.[12,13,15,16] Due to the topology of the "pinecones" (Fig 1) and the potential loss of intracrystalline protein material during FIB sectioning (Fig 2),[12,13,15,16] we are presently unable to directly visualize protein phases either on or within mineral crystals using SEM. Nonetheless, we believe that the formation of these ordered nanoporosities may have occurred in the following manner: a) nanoporosity formation was initiated during a specific period of mineral growth when protein aggregates were in substantial contact with the forming amorphous mineral surface and slowed the nucleation process at the mineral surface;[12,13,15] b) Subsequently, as mineral overgrowth covered these phases, the mineralization process "recovered" and

the protein aggregates became entrapped within the mineral phase and subsequently formed intracrystalline voids or nanopores that were concentrated at the formerly exposed interface.[12] Additional studies will be required to understand the process of annular nanopore formation within calcite crystals.

Under low ionic strength and mineralization-relevant conditions, the formation of protein phases or hydrogels by 1:1 cAP7 : rPFMG1 is significant (Figs 4, 5) and does not directly correlate in dimension or morphology with the protein phases formed individually by cAP7 nor rPFMG1. These results suggest that cAP7 and rPFMG1 protein molecules may be interacting with each other under these conditions, forming heteroaggregates of some kind. Direct evidence of protein-protein interactions under low ionic strength and Ca(II) conditions are observed in our QCM-D experiments (Fig 6). When either protein is adsorbed onto poly-L-Lys coated Au chips, there is a detectable interaction between the adsorbent and the flowcell-introduced protein under aqueous conditions (Fig 6; Figs S6, S7, Supporting Information), and these interactions intensify by a factor of 2 in the presence of Ca(II) ions (Fig 6). Given that each protein originates from different nacre tissues (AP7, shell nacre; PFMG1, pearl nacre) and different organisms (AP7 = gastropod; PFMG1 = oyster), intermolecular interactions between both proteins was unexpected. However, note that both proteins feature combinations of intrinsically disordered[48-52] and cross-beta strand amyloid-like aggregation-prone[52-55] sequences; these well-documented putative sites for protein-protein interaction (Fig S1, Supporting Information).[14,18] Hence, if both proteins possess these highly interactive sequences, then there exist sufficient driving forces that would promote non-specific interactions between cAP7 and rPFMG1 irregardless of their tissue or phylogenetic origins (Figs 4-6). In the presence of Ca(II)(Fig 6), we believe that these non-specific interprotein interactions intensify as a result of salting out / charge neutralization effects at Asp and Glu residues which make rPFMG1 and cAP7 more insoluble in

aqueous media and thus promotes hydrophobic-hydrophobic interactions between the proteins. Thus, in aqueous media (Fig 4) or on surfaces (Fig 5, 6), we believe that the two proteins co-aggregate together and form a hybrid protein phase or hydrogel that influences the outcome of the nucleation (Figs 3,4) and crystal growth (Figs 1, 2) processes in a synergistic fashion.

Finally, we would like to discuss the ramifications of combinatorial protein studies with regard to probing and understanding the biomineralization process. Clearly, much of our current understanding of the biomineralization process has been obtained from three kinds of studies: a) *in vitro* studies using protein analogs (e.g., polymers, additives, small molecules);[30-40] b) *in vitro* studies that employ individual proteins;[12-19;44] c) *in situ* studies of protein components within extracellular matrices.[20-29] All of these approaches are valid, yet in many cases these studies cannot offer insights into synergistic macromolecular-guided nucleation and crystal growth processes, e.g., the interaction or cooperativity between two or more organic components and the impact of this synergy on the biomineralization process. We believe that a combinatorial approach using two or more well-characterized biomineralization proteins can probe this synergy aspect by providing a defined environment for examining, testing, and manipulating multiple macromolecular components on a proportionality (i.e., ratios, Figs 1-6) or temporal (i.e., timed introduction of one or more components, Figs 4, 6) basis within a defined mineralization setting. We believe that his approach, when partnered with other studies, will provide a better understanding of how proteins or additive regulate mineral formation.

ASSOCIATED CONTENT

Supporting Information. AP7 and PFMG1 primary sequences (Figure S1), SEM images of calcitic pinecone morphologies generated by 1:1 cAP7 : rPFMG1 (10 μM : 10 μM)(Fig S2); MicroRaman

spectra and assignments for calcium carbonate crystals formed in the presence of 1:1 cAP7 : rPFMG1 (Figure S3, Table S1); calcium potentiometric titration data for cAP7, rPFMG1, and cAP7 : rPFMG1 mixtures (Figure S4, S5, Table S2); QCM-D data for cAP7 : rPFMG1 = 1:1 (Figure S6, S7).

This material is available free of charge via the Internet at http://pubs.acs.org.

AUTHOR INFORMATION

Corresponding Author

*To whom correspondence should be addressed: John Spencer Evans, Laboratory for Chemical Physics, Division of Basic Sciences and Center for Skeletal Biology, New York University College of Dentistry, 345 E. 24th Street, New York, NY, 10010. Tel.:   (212) 998-9605; Fax: (212) 995-4087. Email: jse1@nyu.edu.

Present Addresses

[1]Currently with Albert Einstein College of Medicine, Bronx, NY, USA
[2]Currently with Department of Chemistry, Simon Fraser University, Burnaby, Canada.

Author Contributions

The manuscript was written through contributions of all authors. All authors have given approval to the final version of the manuscript.

microRaman studies made use of the Cornell Center for Materials Research Shared Facilities (NSF MRSEC DMR-1120296).

ABBREVIATIONS

STEM = scanning transmission electron microscopy, cAP7 = chemical synthesized aragonite protein 7, Haliotis rufescens; rPFMG1 = recombinant Pinctada fucata mantle gene 1; QCM-D = quartz crystal microbalance with dissipation monitoring; PNC = prenucleation cluster; ACC = amorphous calcium carbonate; FIB = focused ion beam sectioning.

REFERENCES

[1] Bezares, J., Asaro, R.J., Hawley, M. (2010) Macromolecular structure of the organic framework of nacre in Haliotis rufescens: Implications for mechanical response. J. Struct. Biol. 170, 484-500.

[2] Addadi, L., Joester, D., Nudelman, F., Weiner, S. (2006) Mollusk shell formation: A source of new concepts for understanding the biomineralization process. Chem Eur. J. 12, 980-987.

[3] Studart, A.R. (2012) Towards high-performance bioinspired composites. Adv. Materials 24, 5024-5044.

[4] Wegst, U.G.K., Bai, H., Saiz, E., Tomsia, A.P., Ritchie, R.O. (2015) Bioinspired materials. Nature Materials 14, 23-36.

[5] Sun, J., Bhushan, B. (2012) Hierarchical structure and mechanical properties of nacre: A review. RSC Adv. 2, 7617-7632.

[6] Zhang, G., Li, X. (2012) Uncovering aragonite nanoparticle self-assembly in nacre – A natural armor. Cryst. Growth Design 12, 4306-4310.

[7] Li, X., Chang, W.C., Chao, Y.J., Wang, R., Chang, M. (2004) Nanoscale structural and mechanical characterization of a natural nanocomposite material: The shell of red abalone. NanoLetters 4, 613-617.

[8] Li, X., Huang, Z. (2009) Unveiling the formation mechanism of pseudo-single-crystal aragonite platelets in nacre. Phys. Rev. Lett. 102, 075502-075506.

[9] Zheng, G., Xu, J. (2013) From colloidal nanoparticles to a single crystal: New insights into the formation of nacre's aragonite tablets. J. Struct. Biol. 182, 36-43.

[10] Checa, A.G., Cartwright, J.H.E., Willinger, M.G. (2011) Mineral bridges in nacre. J. Struct. Biol. 176, 330-339.

[11] Xia, S., Wang, Z., Chen, H., Fu, W., Wang, J., Li, Z., Jiang, L. (2015) Nanoasperity: Structure origin of nacre-inspired nanocomposites. ACS Nano 9, 2167-2172.

[12] Chang, E.P., Evans, J.S. (2015) Pif97, a von Willebrand and Peritrophin biomineralization protein, organizes mineral nanoparticles and creates intracrystalline nanochambers. Biochemistry 54, 5348-5355.

[13] Chang, E.P., Williamson G., Evans, J.S. (2015) Focused ion beam tomography reveals the presence of micro-, meso-, and macroporous intracrystalline regions introduced into calcite crystals by the gastropod nacre protein AP7. Crystal Growth and Design 15, 1577-1582.

[14] Perovic, I., Chang, E.P., Verch, A., Rao, A., Cölfen, H., Kroeger, R., Evans, J.S. (2014) An oligomeric C-RING nacre protein influences pre-nucleation events and organizes mineral nanoparticles. Biochemistry 53, 7259-7268.

[15] Chang, E.P., Russ, J.A., Verch, A., Kroeger, R., Estroff, L.A., Evans, J.S. (2014) Engineering of crystal surfaces and subsurfaces by an intracrystalline biomineralization protein. Biochemistry 53, 4317-4319.

[16] Chang, E.P., Russ, J.A., Verch, A., Kroeger, R., Estroff, L.A., Evans, J.S. (2014) Engineering of crystal surfaces and subsurfaces by framework biomineralization protein phases. Cryst.Eng. Commun. 16, 7406-7409.

[17] Perovic, I., Chang, E.P., Lui, M., Rao, A., Cölfen, H., Evans, J.S. (2014) A framework nacre protein, n16.3, self-assembles to form protein oligomers that participate in the post-nucleation spatial organization of mineral deposits. Biochemistry 53, 2739-2748.

[18] Perovic, I., Mandal, T., and Evans, J.S. (2013) A pseudo EF-hand pearl protein self-assembles to form protein complexes that amplify mineralization. Biochemistry 52, 5696-5703.

[19] Chang, E.P., Perovic, I., Rao, A., Cölfen, H., Evans, J.S. (2016) Insect cell glycosylation and its impact on the functionality of a recombinant intracrystalline nacre protein, AP24. Biochemistry, in press, DOI: 10.1021/acs.biochem.5b01186

[20] Suzuki, M., Iwashima, A., Kimura, M., Kogure, T., Nagasawa, H. (2013) The molecular evolution of the Pif family proteins in various species of mollusks. Mar Biotech. 15, 145-158.

[21] Zhang, G., et al., (2012) The oyster genome reveals stress adaptation and complexity of shell formation. Nature 490, 49-54.

[22] Fang, D., Xu, G., Hu, Y., Pan, C., Xie, L., Zhang, R. (2011) Identification of genes directly involved in shell formation and their functions in pearl oyster, Pinctada fucata. PLOS One 6, 1-13.

[23] Gardner, L.D., Mills, D., Wiegand, A., Leavesley, D., Elizur, A. (2011) Spatial analysis of biomineralization associated gene expression from the mantle organ of the pearl oyster, Pinctada maxima. BMC Genomics 12, 455-470.

[24] Xiang, L., Su, J., Zheng, G., Liang, J., Zhang, G., Wang, H., Xie, L., Zhang, R. (2013) Patterns of expression in the matrix proteins responsible for nucleation and growth of aragonite crystals in flat pearls of Pinctada fucata. PLOS One 8, e66564, doi:10.1371/journal.pone.0066564.

[25] Jackson, D.J., McDougall, C., Woodcroft, B., Moase, P., Rose, R.A., Kube, M., Reinhart, R., Rokhsar, D.S., Montagnani, C., Joube, C., Piquemal, D., Degnan, B.M. (2010) Parallel evolution of nacre building gene sets in mollusks. Mol. Biol. Evol. 27, 591-608.

[26] Marie, B., Joubert, C., Tayale, A., Zanella-Cleon, I., Belliard, C., Piquemal, D., Cochennec-Laureau, N., Marin, F., Gueguen, Y., Montagnani, C. (2012) Different secretory repertoires control the biomineralization processes of prism and nacre deposition of the pearl oyster shell. Proc. Natl. Acad. Sci USA 109, 20986-20991.

[27] Thompson, J.B., Paloczi, G.T., Kindt, J.H. Michenfelder, M., Smith, B.L., Stucky, G., Morse, D.E., Hansma, P.K. (2000) Direct observation of the transition from calcite to aragonite growth induced by abalone shell proteins. Biophys. J. 79, 3307-3312.

[28] Xiang, L., Su, J., Zheng, G., Liang, J., Zhang, G., Wang, H., Xie, L., Zhang, R. (2013) Patterns of expression in the matrix proteins responsible for nucleation and growth of aragonite crystals in flat pearls of Pinctada fucata. PLOS ONE 6, e66564, 1-9.

[29] Falini, G., Albeck, S., Weiner, S., Addadi, L. (1996) Control of aragonite or calcite polymorphism by mollusk shell macromolecules. Science 271, 67-69.

[30] Gebauer, D., Kellermeier, M., Gale, J.D., Bergstrom, L., Cölfen, H. (2014) Pre-nucleation clusters as solute precursors in crystallization. Chem. Soc. Rev. 43, 2348-2371.

[31] Gebauer, D., Volkel, A., Cölfen, H. (2008) Stable prenucleation of calcium carbonate clusters. Science 322, 1819-1822.

[32] Gebauer, D., Cölfen, H. (2011) Prenucleation clusters and non-classical nucleation. Nano Today 6, 564-584.

[33] Demichelis, R., Raiteri, P., Gale, J.D., Quigley, D., Gebauer, D. (2011) Stable prenucleation mineral clusters are liquid-like ionic polymers. Nature Commun. 2, 1-8.

[34] Gebauer, D., Cölfen, H., Verch, A., Antonietti, M. (2008) The multiple roles of additives in CaCO3 crystallization: A quantitative case study. Adv. Mat. 21, 435-439.

[35] Verch, A., Gebauer, D., Antonietti, M., Cölfen, H. (2011) How to control the scaling of CaCO3: a "fingerprinting technique" to classify additives. Phys. Chem. Chem. Phys. 13, 16811−16820.

[36] Kellermeier, M., Cölfen, H., Gebauer, D. (2013) Investigating the early stages of mineral precipitation by potentiometric titration and analytical ultracentrifugation. in Research Methods in Biomineralization Science. Ed. By De Yoreo, J.J. Book Series: Methods in Enzymology 532, 45-69.

[37] Rao, A., Berg, J.K, Kellermeier, M., Gebauer, D. (2014) Sweet on biomineralization: Effects of carbohydrates on the early stages of calcium carbonate crystallization. European Journal of Mineralogy 26, 537-544.

[38] Picker, A., Kellermeier, M., Seto, J., Gebauer, D., Cölfen, H, (2012) The multiple effects of amino acids on the early stages of calcium carbonate crystallization. Zeitschrift für Kristallographie 227, 744-753.

[39] Li, H., Estroff, L.A. (2009) Calcite growth in hydrogels: Assessing the mechanism of polymer-network incorporation into single crystals. Adv Mat. 21, 470-473.

[40] Li, H.Y.; Xin, H.L.; Muller, D.A.; Estroff, L.A. (2009) Visualizing the 3D internal structure of calcite single crystals grown in agarose hydrogels. Science 326, 1244-1247.

[41] Gries, K., Kröger, R., Kübel, C., Fritz, M., Rosenauer, A. (2009) Investigations of voids in the aragonite platelets of nacre. Acta Biomaterialia 5, 3038–3044.

[42] Bewernitz, M.A., Gebauer, D., Long, J., Colfen, H., Gower, L.B. (2012) A metastable liquid precursor phase of calcium carbonate and its interactions with polyaspartate. Faraday Discussions 159, 291-312.

[43] Amos, F.F., Sharbaugh, D.M., Talham, D.R., Gower, L.B. (2007) Formation of single-crystalline aragonite tablets/films via an amorphous precursor. Langmuir 23, 1988-1994.

[44] Wolf, S.E., Leiterer, J., Pipich, V., Barrea, R., Emmerling, F., Tremel, W. (2011) Strong stabilization of amorphous calcium carbonate emulsion by ovalbumin: Gaining insight into the mechanism of 'polymer-induced liquid precursor' processes. J. Am. Chem. Soc. 133, 12642-12649.

[45] Gower, L.B. (2008) Biomimetic model systems for investigating the amorphous precursor pathway and its role in biomineralization. Chem. Rev. 108, 4551-4627.

[46] Li, M., Ran, X., Fang, M., Shi, J., Qin, H., Goh, J.M., Song, J. (2006) Resurrecting abandoned proteins with pure water: CD and NMR studies of protein fragments solubilized in salt-free water. Biophys. J. 91, 4201-4209.

[47] Richter, R., Mukhopadhyay, A., Brisson, A. (2003) Pathways of lipid vesicle deposition on solid surfaces: A QCM-D and AFM study. Biophys. J. 85, 3035-3047.

[48] Lee, R. van der., et al., (2015) Classification of intrinsically disordered regions and proteins. Chem. Rev. 114, 6489-6631.

[49] Uversky, V.N., Dunker, A.K. (2010) Understanding protein non-folding. Biochem. Biophys. Acta 1804, 1231-1264.

[50] Uversky, V.N., Dunker, A.K. (2012) Multiparametric analysis of intrinsically disordered proteins: Looking at intrinsic disorder through compound eyes. Anal. Chem. 84, 2096-2104.s

[51] Uversky, V.N., Gillespie, J.R., Fink, A.L. (2000) Why are natively unfolded proteins unstructured under physiologic conditions? Proteins: Structure, Function, Genetics 41, 415-427.

[52] Evans, J.S. (2012) Identification of intrinsically disordered and aggregation - promoting sequences within the aragonite-associated nacre proteome, Bioinformatics 28, 3182-3185.

[53] Garbuzynskiy, S.O., Lobanov, M.Y., Galzitskaya, O.V. (2010) FoldAmyloid: A method of prediction of amyloidogenic regions from protein sequence. Bioinformatics 26, 326-332.

[54] Conchillo-Sole, O., de Groot, N.S., Aviles, F.X., Vendrell, J., Daura, X., Ventura, S. (2007) AGGRESCAN: a server for the prediction and evaluation of "hot spots" of aggregation in polypeptides, BMC Bioinformatics 8, 65-82.

[55] Goldschmidt, L., Teng, P.K., Riek, R., Eisenberg, D. (2010) The amylome, all proteins capable of forming amyloid-like fibrils. Proc. Natl. Acad. Sci USA 107, 3487-3492.
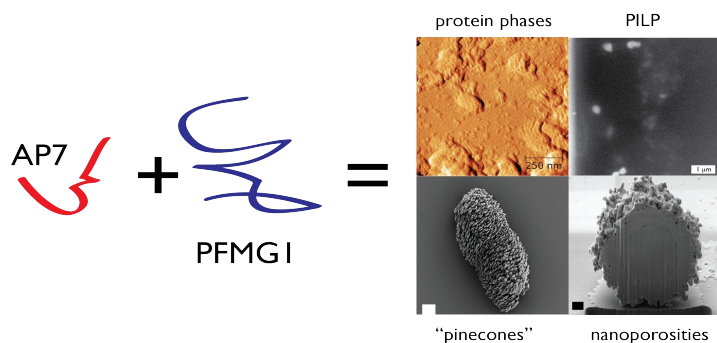
Table of Contents (TOC) Figure